



Simpson, N., & Mellor, P. H. (2017). Additive manufacturing of shaped profile windings for minimal AC loss in gapped inductors. In *2017 IEEE International Electric Machines and Drives Conference (IEMDC 2017)* Institute of Electrical and Electronics Engineers (IEEE).
<https://doi.org/10.1109/IEMDC.2017.8002337>

Peer reviewed version

Link to published version (if available):
[10.1109/IEMDC.2017.8002337](https://doi.org/10.1109/IEMDC.2017.8002337)

[Link to publication record in Explore Bristol Research](#)
PDF-document

This is the author accepted manuscript (AAM). The final published version (version of record) is available online via IEEE at <http://ieeexplore.ieee.org/document/8002337/>. Please refer to any applicable terms of use of the publisher.

University of Bristol - Explore Bristol Research

General rights

This document is made available in accordance with publisher policies. Please cite only the published version using the reference above. Full terms of use are available:
<http://www.bristol.ac.uk/pure/about/ebr-terms>

Additive Manufacturing of Shaped Profile Windings for Minimal AC Loss in Gapped Inductors

Nick Simpson¹ and Phil H. Mellor¹

¹Department of Electrical and Electronic Engineering, University of Bristol, Bristol, UK, nick.simpson@bristol.ac.uk

Abstract—Wound components typically represent approximately 50 % of the total mass of a power converter, consequently minimising the mass and volume of transformers and filter inductors is an important challenge in the design of compact power dense converters in transport and other demanding applications. The research described in this paper contributes to a body of work investigating design tools and new manufacturing processes aimed at reducing the mass and volume of wound components. In this instance, the design and manufacture of minimal AC loss shaped profile windings using metal additive manufacturing is explored. A prototype inductor is manufactured and experimentally tested to demonstrate the advantages of shaped windings for AC loss reduction.

Index Terms—AC loss, wound passive component, additive manufacturing, copper

I. INTRODUCTION

Wound passive components are a necessary part of a power electronic system, however, they typically represent approximately 50 % of the total mass of a power converter and contribute significantly to losses and volume, [1], [2]. Consequently, in automotive and aerospace applications where mass and space are at a premium it is desirable to minimise the mass and volume of transformers and filter inductors, [3].

The fringing electromagnetic field around the gap in a gapped inductor core tends to interact with the winding conductors and significantly increase the AC loss, Fig. 3, above that attributed to conductor level skin and proximity effects, [4], [5]. Hence, it is a common design challenge to arrange the conductors to minimise interaction with the fringing field by shifting or shaping the winding cross-section within the winding window. Minimising fringing loss effects can lead to more compact and efficient inductor designs as the windings can be operated at higher net current densities within a given thermal constraint, [6]. Hence, a route to volume and mass reduction is the minimisation of winding loss.

Shaped windings have been achieved using round wire bundles wound on to forming bobbins, [7] or by the use of pre-cut foil windings in a barrel wound configuration to form notches in appropriate locations, [8], [9]. Shaped planar windings have been produced for high current applications using Printed Circuit Boards (PCB) or solid conductor busbar arrangements, [4], [10]–[12]. However, the PCB and busbar implementations require interconnects between the discrete layers in the end-windings which adds complexity to their manufacture and increases the packaging envelope.

In this paper, the use of metal Additive Manufacturing (AM), [13], to produce a single piece shaped profile helical

winding for an 80 μH , 200 A_{RMS} , 400 Hz gapped inductor is explored. The inductor is designed to meet the specification set out in Table I. The bespoke core is sized using a combination of the area product method, [14], and a geometric parameter sweep to identify an optimal core aspect ratio, [15]. Within this fixed winding window, a conductor shape optimisation is performed to investigate the effect of varying the conductor geometry on the AC winding loss. A minimal AC loss winding design is identified and manufactured using Direct Metal Laser Sintering (DMLS) in a copper alloy material. The inductor is experimentally tested to verify the modelling results and to demonstrate the potential of AM in the design and production of low AC loss windings with a high degree of geometric freedom.

TABLE I
INDUCTOR SPECIFICATION

Parameter	Value	Unit
Active length, l_{act}	80	mm
DC winding resistance, R_{DC}	1	m Ω
DC winding power loss, P_{DC}	40	W
Electrical resistivity, ρ	1.72×10^{-8}	$\Omega \cdot \text{m}$
Peak flux density, \hat{B}	1.2	T
Peak current, \hat{I}	283	A
Packing factor, PF	75	%
Inductance, L	80	μH
Number of turns, N	8	n/a
Operating frequency, f	400	Hz

II. INDUCTOR CORE SIZING

The inductor core is sized using the area product method, [14], (1), where A_c , A_w and \bar{l} are geometric quantities describing the necessary area of the core, area of the winding window and the mean length of a winding turn respectively. The resistivity ρ , target inductance L , peak current \hat{I} , peak core flux density \hat{B} , DC winding resistance R_{DC} and the packing factor PF are given in Table I. In the present study, thermal aspects of the design are neglected, hence a low DC winding resistance is selected and the inductor is assumed to be mounted to a water cooled cold plate. An 8 turn, single conductor winding is assumed in order to simplify the electrical insulation process at the manufacturing stage, section V.

$$\frac{A_c^2 A_w}{\bar{l}} \geq \frac{\rho L^2 \hat{I}^2}{\hat{B} R_{DC} PF} \quad (1)$$

A geometric parameter sweep is performed using 2D Finite Element Analysis (FEA) to identify the aspect ratio of the core which results in minimal AC loss at 400 Hz. The model assumes a uniform winding in which each of the conductors have equal height and width as illustrated in, Fig. 3. The AC winding loss is plotted as a function of core aspect ratio in Fig. 1 where a minimum exists between 1.6 and 2.4, [15]. An aspect ratio of 1.67 is selected which yields a nominal conductor height of 2.75 mm. An initial air-gap length, l_g of 2.2 mm is found using (2) where A_c is the cross sectional area of the core. Since (2) neglects the fringing field around the air-gap and the non-linearity of the core, 2D FEA is used to tune the air-gap length in order to achieve an inductance of 80 μ H. A schematic of the resulting core geometry is illustrated in Fig. 2.

$$l_g = \frac{\mu_0 L \hat{I}^2}{\hat{B}^2 A_c} \quad (2)$$

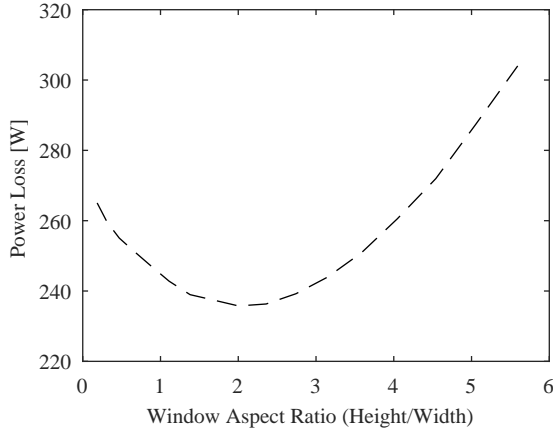


Fig. 1. Winding AC loss as a function of core window aspect ratio.

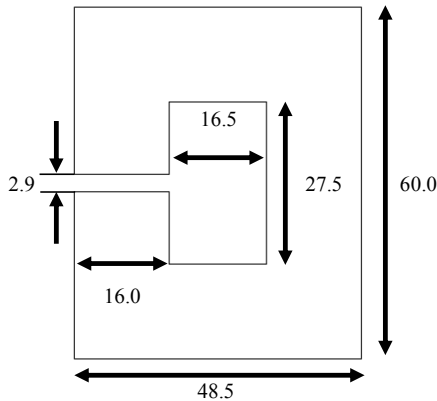


Fig. 2. Inductor core geometry (one half shown), dimensions in mm.

III. WINDING DESIGN STUDY

Given the fixed winding window, air-gap length (determined using 2D FEA), number of turns, N and packing factor, PF , the conductor dimensions and position can be varied in order to minimise the interaction between the air-gap fringing field and the winding conductors to minimise AC winding loss, [11], [16].

A number of analytical methods exist to predict AC winding losses in round and rectangular conductors, [17]–[20], and in the presence of an air-gap, [5]. Extended methods able to cater for arbitrary current waveforms are reported in [20], [21]. These modelling methods have been successfully applied to AC winding loss prediction of shaped foil windings, [16], [22] and shaped helical windings, [4], [11]. However, analytical methods can be time consuming to implement and often have limitations on conductor geometry and applicability in the case of core saturation, [20].

In this study, the inductor is modelled using a parametric 2D FEA model, [23], which includes the effects of winding eddy currents and non-linearity of the core permeability. The conductor dimensions are varied automatically using a Particle Swarm Optimisation (PSO) algorithm with an objective of minimising AC loss at a fixed frequency of 400 Hz, Table I. The model calculates the AC loss within the active length and assumes that the end-windings are semi-circular with DC loss only.

Four cases of conductor geometry are considered:

- Uniform width and height conductors, (UW, UH), Fig. 3
- Fixed width, variable height conductors, (FW, VH), Fig. 4
- Variable width, fixed height conductors, (VW, FH), Fig. 5
- Variable width and height conductors, (VW, VH), Fig. 6

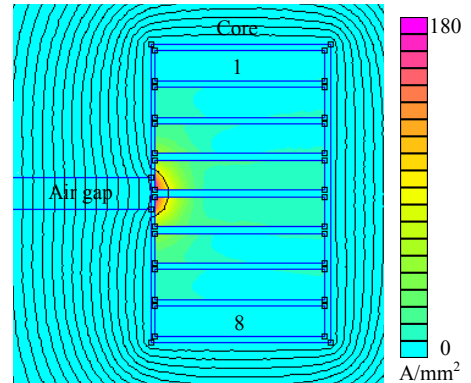


Fig. 3. Current density distribution, uniform width, uniform height conductors.

Winding shape optimisation is performed for each of the conductor geometry configurations, (FW, VH), (VW, FH) and (VW, VH). The conductor dimensions are normalised to the winding window and are assumed to fill the window vertically with a packing factor of 85 %. The width of the conductors are allowed to vary under the assumption that the conductors are abutted to the outer window away from the air-gap. The winding is assumed to be symmetric since the core and fringing field are symmetric. Constraints are not applied to

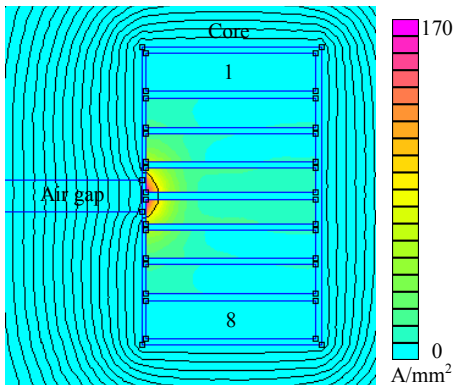


Fig. 4. Current density distribution, fixed width, variable height conductors.

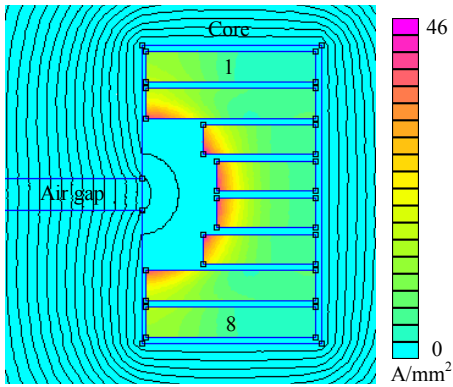


Fig. 5. Current density distribution, variable width, fixed height conductors.

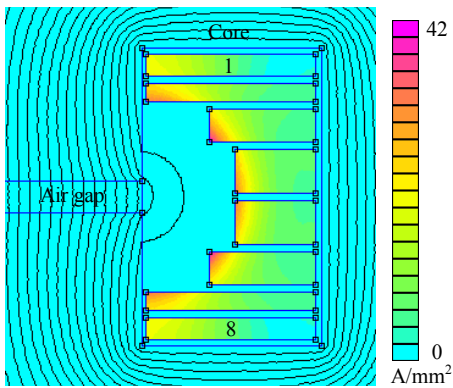


Fig. 6. Current density distribution, variable width, variable height conductors.

the conductor cross section, hence, each conductor geometry is independent and sized based on the global objective of minimising AC loss at 400 Hz. Figs. 3 to 6 show that the peak current density within each conductor reduces as the conductors are moved away from the air-gap fringing field, as expected. Figs. 7 and 8 show the DC and AC losses of each conductor configuration compared with those of the baseline uniform width, uniform height winding, (UW,UH), Fig. 3. Only winding layers 1 to 4 are shown since the AC loss distribution is symmetric.

Allowing the height of the conductors to vary, (FW,VH), Fig. 4, increases the total DC loss by 2.5% due to a reduction

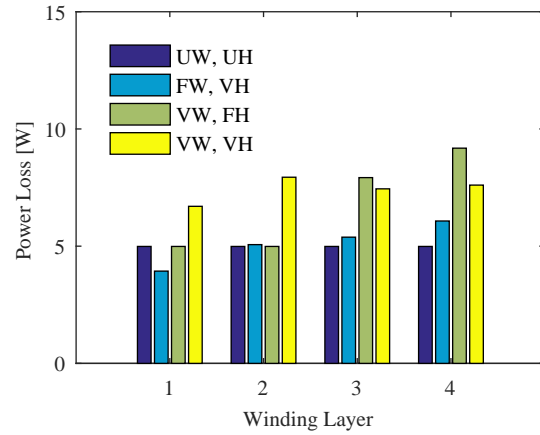


Fig. 7. DC winding loss comparison.

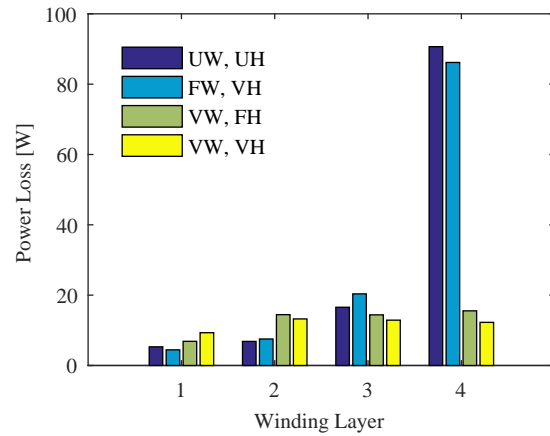


Fig. 8. AC winding loss comparison at 400 Hz.

in cross sectional area, Fig. 7, however, the AC loss is reduced by 0.7 %. Allowing the conductor width to vary, (VW,FH), Fig. 5, has a more significant impact on loss reduction as the conductors are physically moved away from the region of high fringing flux, Fig. 5. In this case the DC loss is increased over the baseline by 35 % due to the diminished cross sectional area, however, the AC loss is reduced by 57 % and the maximum current density reduces from 180 A/mm², Fig. 4, to 46 A/mm², Fig. 5. Combining variable width and height, (VW, VH), Fig. 6, results in a DC loss increase of 39 %, however, the AC loss is reduced by 75 % compared to the baseline design and the losses are distributed more evenly over the conductors with a standard deviation of 1.8 W as opposed to 40.8 W in the baseline case. The distribution and magnitude of the losses influence the temperature profile and hot-spot location of the winding, [23]. Hence, the (VW, VH) winding could result in a lower peak to average temperature and improved reliability. As illustrated in Fig. 6 the current density, and hence loss density within each conductor is concentrated on the conductor edges in closest proximity to the air-gap fringing field.

IV. SHAPED END-WINDINGS

As the winding is to be manufactured using AM, the limitations on geometry, maximum aspect ratios and minimum bend radii suffered by traditionally drawn and edge-wound rectangular conductors are relaxed. Inductor end-windings are typically semi-circular, Fig. 9, however, the end-windings can be shaped to minimise path length and thereby loss, Fig. 10. In addition end-winding shaping can be used to reduce the packaging envelope and consequently increase the overall energy density of the inductor.

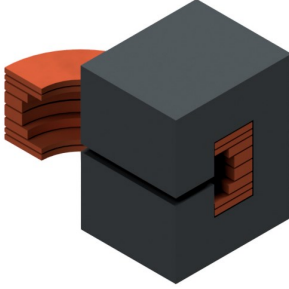


Fig. 9. Semi-circular end-windings.

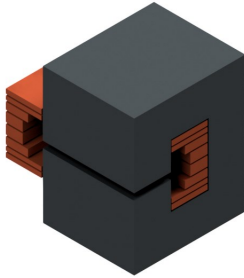


Fig. 10. Semi-square end-windings.

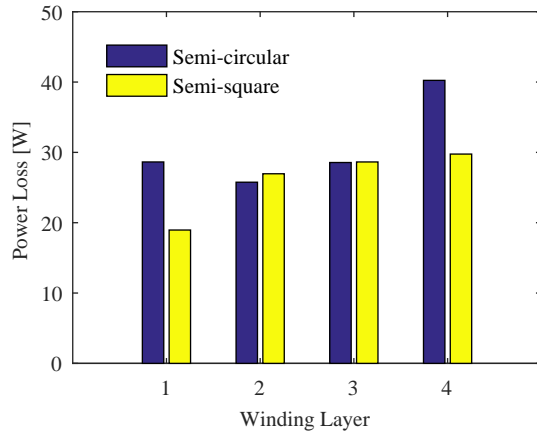


Fig. 11. Total AC winding loss comparison at 200 A_{RMS} and 400 Hz.

The (VW, VH) winding, Fig. 6 is modelled assuming semi-circular end windings using 3D FEA in order to account for the AC loss in the end-windings, Fig. 9. The total AC winding loss predicted using 3D FEA is 23 % higher than that predicted by 2D FEA since the 2D model assumes DC loss only in the end-windings. The end-windings are shaped into a semi-square, Fig. 10, to reduce the effective path length. The separation between each conductor and the air-gap in the active length is maintained in the end-winding to minimise AC loss. Shaping the end-windings reduces the overall AC loss by 15 % to 104 W at 400 Hz and 200 A_{RMS} , as illustrated in Fig. 11.

V. PROTOTYPE INDUCTOR MANUFACTURE

The inductor core is constructed using pre-coated non-grain oriented NO20 SiFe electrical steel laminations bonded into stacks and then cut to shape using Electrical Discharge Machining (EDM).

The 8-turn winding is manufactured from a copper alloy using DMLS. The DMLS process uses a high intensity energy source to selectively sinter powdered metal material in a 2D scan. Further layers of powder are then deposited on top of the sintered layer and the process is repeated to incrementally build a 3D metal part, [13], [24]. The completed part is removed from the powder bed and excess powder recycled before it is separated from the metallic build platform using EDM. The part is then post-baked to enhance the diffusion process between particles, reduce the overall porosity and improve the structure of the part, Fig. 12. The process used has a minimum feature size of 0.5 mm and a dimension tolerance of ± 0.2 mm on features up to 100 mm and ± 0.2 % on features up to 250 mm. A surface roughness of less than $R_a \leq 15$ μm is achieved.

Synthite AC-43 air-drying polyester varnish is used to electrically insulate the winding. In order to ensure a high integrity, even coating, the winding is mounted to an aluminium block via the terminals to separate the winding layers, Fig. 13. The varnish is then drip fed onto the coil as it rotates on a DC motor driven fixture. Once covered the fixture is transferred to an oven and the insulation is cured at 75°C for 60 minutes under constant rotation.



Fig. 12. Copper coil with non-uniform conductor profiles produced using a DMLS additive manufacturing process.

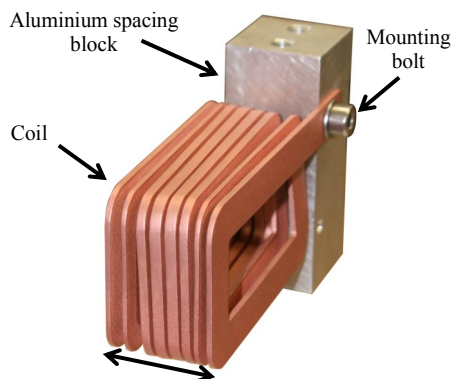


Fig. 13. Coil mounted to an aluminium spacing block prior to insulation process.

VI. EXPERIMENTAL TESTING

The inductance of the prototype is measured as $83 \mu\text{H}$ using a small signal Wayne Kerr 6500P LCR meter which is within 4 % of the $80 \mu\text{H}$ specification, Table I. The inductor core was sized assuming a peak flux density of 1.2 T, below saturation of the NO20 SiFe electrical steel, however, the inductance should be measured at the rated current in order to establish the linearity of the component. The core is manufactured in two parts and aligned by semi-circular features to minimise alignment error, Fig. 14.

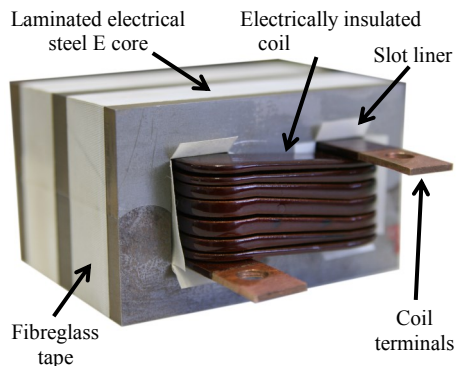


Fig. 14. AM copper winding mounted on the electrical steel core.

The DC and AC losses of the assembled inductor, Fig. 14, are measured by applying DC or AC (sinusoidal waveform) to the winding using a low Total Harmonic Distortion (THD) California Instruments programmable source and measuring the resultant voltage drop and current using a precision Norma 5000 power analyser and a passive Fluke current shunt, Fig. 15.

The AM process used to manufacture the winding remains at an experimental stage. The resulting electrical conductivity of AM parts is a function of the powder composition such as oxide and oxygen content in addition to the AM process variables and post production steps, [25]. The electrical conductivity of the winding was measured as 51% of the International Annealed Copper Standard (IACS) of 58.108 MS/m. Hence, the electrical conductivity of the prototype is less

than that of aluminium (approximately 60% IACS), however, the conductivity is sufficient to demonstrate the advantages that AM and shaped windings can offer to the design of wound passive components. As the electrical conductivity of the AM material was unknown before a prototype winding was manufactured, the winding shape optimisation assumed copper at 100 % IACS, hence the resulting conductor geometry would change if the winding shape optimisation were repeated with updated electrical conductivity data. The 3D FEA was repeated with updated electrical conductivity data to enable a comparison to measured loss data.

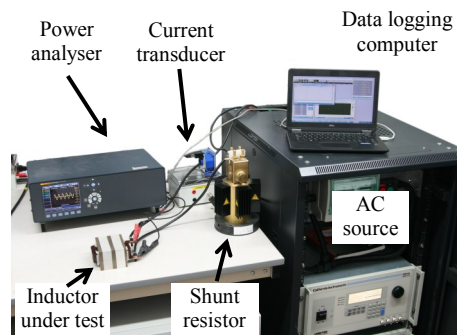


Fig. 15. Experimental apparatus used to measure the inductor losses.

Fig. 16 shows the measured AC loss and that predicted by 3D FEA as a function of frequency for a fixed temperature of 20°C and current of $90 \text{ A}_{\text{RMS}}$. The applied current is limited by the AC source available during experimentation. The measured results include the AC winding loss component and the core loss component. In order to separate the losses, the core loss is predicted using 3D FEA and subtracted from the total measured losses to give the AC winding loss as illustrated in Fig. 16. The measured and predicted losses increase as a function of frequency and are in close agreement up to approximately 400 Hz where the losses begin to diverge and the measured losses are greater than predicted. The discrepancy may be caused by variation in winding or core dimensions, non-uniform physical placement of the winding within the core or underestimation of the core losses.

$$\delta = \sqrt{\frac{1}{\sigma \pi f \mu_0}} \quad (3)$$

The AC loss of the baseline (UW, UH) winding, Fig. 3 and the shaped (VW, VH) winding, Fig. 6 are calculated as a function of frequency using 3D FEA assuming 100% IACS representative of copper used in electrical applications and 51% IACS representative of the AM copper, Fig. 17. At 400 Hz the baseline 51% IACS winding exhibits an AC loss of 63 W which is 2.5 times greater than the shaped 51% IACS winding. The large difference in AC loss is due to the air-gap fringing field interacting with the conductors and generating additional eddy current losses as illustrated in Fig. 3. The DC loss of the baseline winding at 100% IACS is approximately

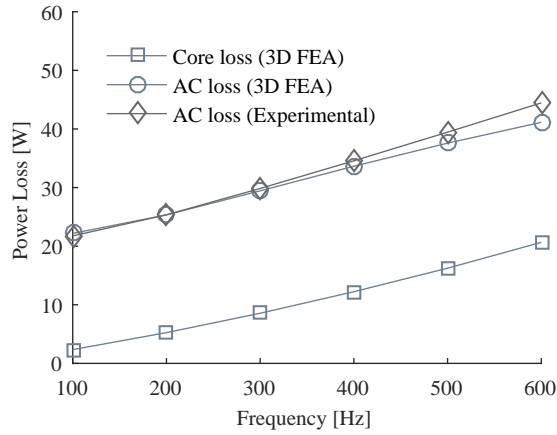


Fig. 16. Predicted and measured AC winding loss.

50% that of the baseline winding at 51% IACS, as expected. However, the difference in AC loss between the baseline winding at 100% IACS and 51% IACS is approximately 5% at 400 Hz since the dominant loss source is the interaction between the air-gap fringing field and the winding. The skin depth δ is a function of the operating frequency f and material conductivity σ , (3), which leads to a skin depth of 4.6 mm for the 51% IACS material and 3.3 mm for the 100% IACS material at 400 Hz, [26].

The difference in AC loss of the shaped winding at 51% IACS and 100% IACS at 400 Hz is approximately 30% which is a larger proportion than the baseline winding since the dominant loss mechanism is no longer the proximity to the air-gap fringing field, rather skin and conductor-conductor proximity effects. If the AM process were able to achieve 100% IACS, the shaped winding would exhibit 3 times less AC loss than the baseline winding with 100% IACS at 400 Hz. In addition, the loss distribution throughout the winding is more uniform in the shaped winding, Figs. 3 and 6, which would aid a more even temperature distribution and reduce the peak to average temperature.

VII. CONCLUSION

This paper has demonstrated the use of metal AM to produce a shaped helical winding for a gapped inductor with an optimised profile which leads to minimal AC winding loss at the operating point of 400 Hz and 200 A_{RMS}. The benefits of greater geometric freedom in the design process enabling variable conductor heights, widths and compact end-windings have been illustrated. The experimentally measured electrical conductivity of the AM winding is 51% IACS which is lower than that of aluminium. However, the AM process used to manufacture the winding remains at an experimental stage and improvements in conductivity to $\geq 85\%$ IACS are anticipated. Since the electrical conductivity can be altered by the AM process, it could become an important design variable enabling electrical resistivity to be tailored to a particular application on a global winding level or locally through the winding as a function of position. The measured and predicted

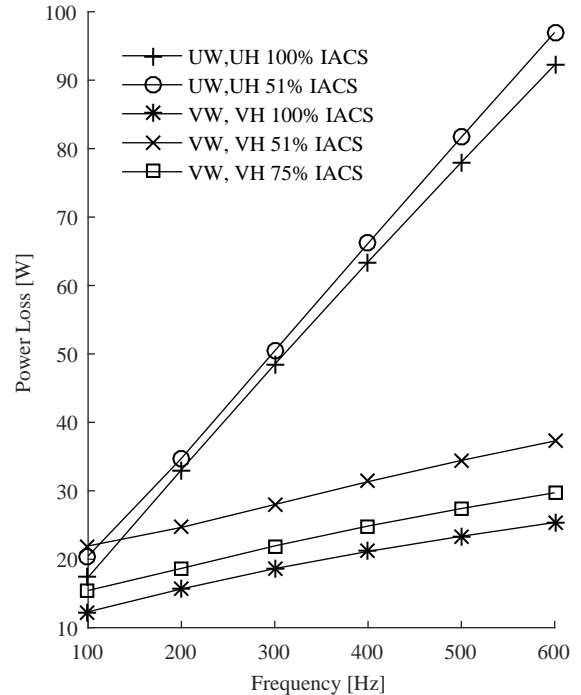


Fig. 17. Comparison of AC winding loss of the baseline (UW, UH) winding and the shaped (VW, VH) winding.

AC winding losses show close agreement which validates the modelling method used. The optimisation process could be made more computationally efficient by the addition of a conductor area constraint ensuring a consistent cross section through the winding. Alternatively, analytical modelling methods could be used to significantly reduce the computational effort and cater for arbitrary current waveforms, [20]. A single layer winding with few turns was selected as a demonstrator in order to simplify the electrical insulation process. The dimensional accuracy of the AM process would allow the production of multilayer windings applicable to electrical machines, transformers and inductors if the electrical insulation could be reliably applied. The AM process is an expensive manufacturing method at present, however, casting technology could be used as an alternative production method with similar geometric freedom, [27], [28]. This paper has demonstrated a significant reduction in AC winding loss through the use of shaped windings. However, due to the complex relationship between the geometry, losses and temperature rise, a coupled thermal and electromagnetic analysis is required to achieve an optimal mass and volume reduction and to give an accurate indication of loss reduction attributable to shaped windings. If the geometric freedom offered by AM methods is to be exploited, tailored enhancements to existing electromagnetic and thermal modelling methods will become an increasingly important area of research.

REFERENCES

- [1] T. E. Salem, D. P. Urciuoli, V. Lubomirsky, and G. K. Ovrebo, "Design considerations for high power inductors in dc-dc converters," in *APEC 07 - Twenty-Second Annual IEEE Applied Power Electronics Conference and Exposition*, Feb 2007, pp. 1258–1263.
- [2] G. Shane and S. Sudhoff, "Design paradigm for permanent magnet inductor-based power converters," in *2015 IEEE Power Energy Society General Meeting*, July 2015, pp. 1–1.
- [3] M. Gerber, J. A. Ferreira, I. W. Hofsjager, and N. Seliger, "A very high density, heatsink mounted inductor for automotive applications," in *Conference Record of the 2002 IEEE Industry Applications Conference. 37th IAS Annual Meeting (Cat. No.02CH37344)*, vol. 2, Oct 2002, pp. 948–954 vol.2.
- [4] D. C. Pentz and I. W. Hofsjager, "A performance evaluation of shaped planar inductor windings in gapped core applications utilizing turns with constant dc-resistance," in *2007 IEEE Power Engineering Society Conference and Exposition in Africa - PowerAfrica*, July 2007, pp. 1–6.
- [5] W. A. Roshen, "Fringing field formulas and winding loss due to an air gap," *IEEE Transactions on Magnetics*, vol. 43, no. 8, pp. 3387–3394, Aug 2007.
- [6] G. Calderon-Lopez, A. J. Forsyth, D. L. Gordon, and J. R. McIntosh, "Evaluation of sic bjts for high-power dc-dc converters," *IEEE Transactions on Power Electronics*, vol. 29, no. 5, pp. 2474–2481, May 2014.
- [7] C. R. Sullivan, J. D. McCurdy, and R. A. Jensen, "Analysis of minimum cost in shape-optimized litz-wire inductor windings," in *2001 IEEE 32nd Annual Power Electronics Specialists Conference (IEEE Cat. No.01CH37230)*, vol. 3, 2001, pp. 1473–1478 vol. 3.
- [8] J. D. Pollock and C. R. Sullivan, "Loss models for shaped foil windings on low-permeability cores," in *2008 IEEE Power Electronics Specialists Conference*, June 2008, pp. 3122–3128.
- [9] —, "Gapped-inductor foil windings with low ac and dc resistance," in *Conference Record of the 2004 IEEE Industry Applications Conference, 2004. 39th IAS Annual Meeting.*, vol. 1, Oct 2004, p. 557.
- [10] T. Nomura, C. M. Wang, K. Seto, and S. W. Yoon, "Planar inductor with quasi-distributed gap core and busbar based planar windings," in *2013 IEEE Energy Conversion Congress and Exposition*, Sept 2013, pp. 3706–3710.
- [11] D. C. Pentz, "Overview of helical foil winding design for planar magnetic components," in *2013 IEEE International Conference on Industrial Technology (ICIT)*, Feb 2013, pp. 628–632.
- [12] K. D. T. Ngo, R. P. Alley, and A. J. Yerman, "Fabrication method for a winding assembly with a large number of planar layers," *IEEE Transactions on Power Electronics*, vol. 8, no. 1, pp. 55–61, Jan 1993.
- [13] W. E. Frazier, "Metal additive manufacturing: a review," *Journal of Materials Engineering and Performance*, vol. 23, no. 6, pp. 1917–1928, 2014.
- [21] W. G. Hurley, E. Gath, and J. G. Breslin, "Optimizing the ac resistance of multilayer transformer windings with arbitrary current waveforms," in *30th Annual IEEE Power Electronics Specialists Conference. Record. (Cat. No.99CH36321)*, vol. 1, Aug 1999, pp. 580–585 vol.1.
- [14] M. K. Kazimierczuk and H. Sekiya, "Design of ac resonant inductors using area product method," in *2009 IEEE Energy Conversion Congress and Exposition*, Sept 2009, pp. 994–1001.
- [15] R. A. Jensen and C. R. Sullivan, "Optimal core dimensional ratios for minimizing winding loss in high-frequency gapped-inductor windings," in *Applied Power Electronics Conference and Exposition, 2003. APEC '03. Eighteenth Annual IEEE*, vol. 2, Feb 2003, pp. 1164–1169 vol.2.
- [16] J. D. Pollock and C. R. Sullivan, "Loss models for shaped foil windings on low-permeability cores," in *2008 IEEE Power Electronics Specialists Conference*, June 2008, pp. 3122–3128.
- [17] P. Wallmeier, "Improved analytical modeling of conductive losses in gapped high-frequency inductors," *IEEE Transactions on Industry Applications*, vol. 37, no. 4, pp. 1045–1054, Jul 2001.
- [18] J. A. Ferreira, "Improved analytical modeling of conductive losses in magnetic components," *IEEE Transactions on Power Electronics*, vol. 9, no. 1, pp. 127–131, Jan 1994.
- [19] N. H. Kutkut, "A simple technique to evaluate winding losses including two dimensional edge effects," in *Proceedings of APEC 97 - Applied Power Electronics Conference*, vol. 1, Feb 1997, pp. 368–374 vol.1.
- [20] C. R. Sullivan, "Computationally efficient winding loss calculation with multiple windings, arbitrary waveforms, and two-dimensional or three-dimensional field geometry," *IEEE Transactions on Power Electronics*, vol. 16, no. 1, pp. 142–150, Jan 2001.
- [22] J. D. Pollock and C. R. Sullivan, "Modelling foil winding configurations with low ac and dc resistance," in *2005 IEEE 36th Power Electronics Specialists Conference*, June 2005, pp. 1507–1512.
- [23] N. Simpson, R. Wrobel, and P. H. Mellor, "Multi-physics design of high-energy-density wound components," in *2015 IEEE Energy Conversion Congress and Exposition (ECCE)*, Sept 2015, pp. 3857–3864.
- [24] D. Jacobson and G. Bennett, "Practical issues in the application of direct metal laser sintering," in *Solid Freeform Fabrication Symposium, Austin, TX, Aug, 2006*, pp. 14–16.
- [25] P. Frigola, O. Harrysson, T. Horn, H. West, R. Aman, J. Rigsbee, D. Ramirez, F. Medina, R. Wicker, and E. Rodriguez, "Fabricating copper components," *Advanced Materials & Processes*, p. 20, 2014.
- [26] P. Mellor, R. Wrobel, and N. Simpson, "Ac losses in high frequency electrical machine windings formed from large section conductors," in *2014 IEEE Energy Conversion Congress and Exposition (ECCE)*, Sept 2014, pp. 5563–5570.
- [27] M. Graninger, F. Horch, A. Kock, H. Pleteit, B. Ponick, D. Schmidt, and F. J. Wastmann, "Casting production of coils for electrical machines," in *2011 1st International Electric Drives Production Conference*, Sept 2011, pp. 159–161.
- [28] M. Grninger, F. Horch, A. Kock, M. Jakob, and B. Ponick, "Cast coils for electrical machines and their application in automotive and industrial drive systems," in *2014 4th International Electric Drives Production Conference (EDPC)*, Sept 2014, pp. 1–7.